Calculating the entrance field near a grain boundary in type-II superconductors

Christopher Wilson*

(Dated: September 8, 2012)

In a type-II superconducting cavity, the Bean-Livingston barrier prevents the penetration of flux vortices parallel to the surface. However, this barrier disappears when the applied external field exceeds the entrance field, H_e. By making an analogy with electrostatics, the method of images may be applied to calculate the interaction energy between a flux vortex and cavity wall. In further applying a conformal transformation to this solution, the interaction energy between a vortex and surface defect may further be found. These techniques are used to calculate the vortex entrance field in the presence of a grain boundary, and are considered with respect to using Nb_3Sn in the construction of superconducting accelerators.

I. INTRODUCTION

For the type-II classification of superconductivity, there exists a meta-stable transition state between the normal and Meissner states. A type-II superconductor is characterized by $\kappa > 1/\sqrt{2}$, where the Ginzburg-Landau parameter $\kappa = \lambda/\xi$ is defined as the ratio of the material's London penetration depth λ to it's coherence length ξ. Such values of κ are obtained by Nb_3Sn, with $\kappa \approx 12$, due to its relatively small coherence length. Within this classification of superconductor, it can become energetically favorable for magnetic flux to enter the bulk of a superconducting surface in the form of flux vortices. This occurs when the external applied magnetic field, H_{ext}, is greater than the lower critical field H_{c_1}.

A flux vortex is comprised of of a normal core with radius ξ, as depicted in FIG 1. The amount of flux passing through each vortex is quantized; this is denoted as ϕ_0, a single quantum of magnetic flux. The presence of such vortices are undesirable in radio-frequency applications, as quenching is imminent when magnetic flux penetrates the bulk of an accelerating cavity.

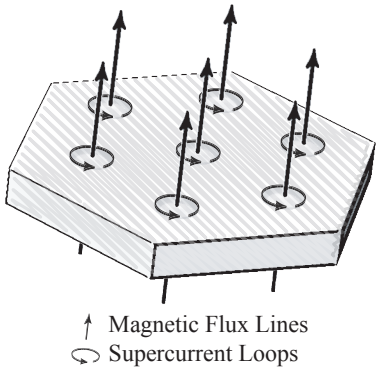

FIG. 1. Lines of magnetic flux encircled by supercurrent, shown penetrating the bulk of a superconducting material. The normal cores within the supercurrent loops have a radius of ξ.

* cwils16@u.rochester.edu

Following [1], a flux vortex in close vicinity to the surface of a superconductor is subjected to an attractive imaging force. This may be conceptualized as the attraction of a vortex to its so called mirror image within the surface, where the fictitious image vortex serves to satisfy boundary conditions associated with the nature of superconductivity. However, flux penetration is ultimately prevented by the Bean-Livingston barrier, which is a function of both the surface geometry and the magnitude of the applied external field. Hence, it follows that the surface geometry also affects the strength of the entrance field, H_e; the maximum achievable external field before flux penetration occurs. From this, it has become well known that surface defects in the form of grain boundaries weaken the entrance field and thus expedite flux penetration. This phenomenon is of particular concern in regards to the limiting implications it has upon using Nb_3Sn as a bulk film within superconducting radio-frequency accelerating cavities.

In this paper, we focus on presenting an in depth work through of the derivation for the entrance field near a grain boundary, as given by Buzdin and Daumens in [2]. We begin by reviewing the mathematical methods used within this derivation, which include several techniques drawn from complex analysis, as well as the method of images from electrostatics. Afterwards, we introduce the vortex-electrostatic analogy and begin our derivation by calculating the vortex-defect attractive imaging force. Following this, the flow of supercurrent around the defect is analyzed. This will allow us to determine the associated Lorentz force acting on the vortex, which will ultimately lead to an analytic expression for the entrance field in the presence of a grain boundary. We follow up these calculations by interpreting the implications they have upon using Nb_3Sn as a superconductor. Finally, we probe the physical accuracy of our choice in grain boundary model by presenting a few insightful results from other work done in this field.

II. MATHEMATICAL FRAMEWORK

In this section, we briefly review the mathematical techniques used throughout the derivation of H_e. In par-

ticular, several techniques from complex analysis will be utilized. A more in-depth treatment of these methods may be found in [3].

A. Forming A Complex Analogy

As we will be working extensively with vectors in a two-dimensional plane, we need to use an analogy to relate this problem from $\mathbb{R}^2$ to one that belongs to the complex plane, $\mathbb{C}$. To accomplish this, we may write a vector $\mathbf{r} = x\hat{i} + y\hat{j}$ in $\mathbb{R}^2$ as $\zeta = x + \imath y$ in $\mathbb{C}$. Furthermore, it follows that the norm of $\mathbf{r}$ is equivalent to the modulus of ζ, such that $|\mathbf{r}| \equiv |\zeta|$. In addition, it is important to also note that a complex function $w = f(\zeta)$ may be interpreted as a mapping from the ζ-plane to the w-plane. This is analogous to that a single real valued function in the form of $y = f(x)$, where a point along the x-axis maps to a point along the y-axis.

B. The Cauchy-Riemann Condition

Having defined the concept of a complex function, it becomes natural to ask whether or not the methods of differential calculus similarly be applied to functions of this type. This is indeed the case, and we define the complex derivative as

$$f'(\zeta) = \lim_{\Delta\zeta \to 0} \frac{f(\zeta + \Delta\zeta) - f(\zeta)}{\Delta\zeta}$$

where we note that the limiting value $f'(\zeta)$ of the difference quotient must be independent of how $\Delta\zeta$ converges to 0. Hence, the value of $f'(\zeta)$ is the same for $\Delta\zeta = \Delta x$ and $\Delta\zeta = i\Delta y$. Then by computing for the real and imaginary parts of $f'(\zeta)$ for each choice of $\Delta\zeta$, respectively, we have

$$f'(\zeta) = \begin{cases} u_x(x,y) + iv_x(x,y), & \text{for } \Delta\zeta = \Delta x \\ v_y(x,y) - iu_y(x,y), & \text{for } \Delta\zeta = \imath\Delta y \end{cases}$$

Therefore, these two values of $f'(\zeta)$ must be identical if f is said to be *analytic* at a point $\zeta \in \mathbb{C}$. Equating the real and imaginary parts above yields the Cauchy-Riemann condition,

$$u_x = v_y \quad \text{and} \quad u_y = -v_x \tag{1}$$

Furthermore, the Cauchy-Riemann condition also provides a useful tool in determining whether or not a vector field is conservative. Consider the complex function $w = u(x,y) + \imath v(x,y)$, here we state without proof that the partial derivatives u_x, u_y, v_x, and v_y are continuous and satisfy the Cauchy-Riemann condition in some region of $\mathbb{C}$ if and only if w is analytic in that region of $\mathbb{C}$. We can further extend this result by noting that a function w is analytic in some region of $\mathbb{C}$ if and only if it satisfies the two-dimensional Laplace Equation

$$\nabla^2 f(\zeta) = 0$$

corresponding to that region in $\mathbb{C}$ [3]. Functions satisfying this equation in the complex plane are said to be *harmonic*. Therefore, it follows that a complex function w is harmonic in some region of $\mathbb{C}$ if and only if it has continuous partial derivatives and satisfies the Cauchy-Riemann condition in that region of $\mathbb{C}$. We make use of this statement in the following development of the complex potential.

C. The Complex Potential

Let $\boldsymbol{v} = v_x\hat{i} + v_y\hat{j}$ be a vector field that satisfies the condition $\nabla \times \boldsymbol{v} = 0$. It then follows from multivariate calculus that $\boldsymbol{v}$ is the gradient of some scalar potential, such that $\boldsymbol{v} = \nabla\Phi$. Now consider $v = v_x + \imath v_y$ to exist in the complex plane, where the same condition is satisfied. We may write

$$v_x = \frac{\partial\Phi}{\partial x} \quad \text{and} \quad v_y = \frac{\partial\Phi}{\partial y}$$

Since Φ is harmonic, it must satisfy the Cauchy-Riemann condition given in (1). Therefore, from the above expression, we may also write

$$v_x = \frac{\partial\Psi}{\partial y} \quad \text{and} \quad v_y = -\frac{\partial\Psi}{\partial x}$$

The functions Φ and Ψ are both harmonic parts of what is referred to as the complex potential

$$\Omega(\zeta) = \Phi + i\Psi \tag{2}$$

From this expression, we note that our original vector field $\boldsymbol{v} \in \mathbb{R}^2$ is analogous to the complex expression of

$$\Omega^{*\prime} = v_x + \imath v_y = v\, e^{\imath\theta} \tag{3}$$

where * denotes the complex conjugate operator.

Additionally, and as further consequence of the Cauchy-Riemann condition, we note that the level sets $\Phi = c_1$ and $\Psi = c_2$ for $c_1, c_2 \in \mathbb{R}$ are mutually orthogonal. This allows for the complex potential to be implemented as a useful tool when dealing with various physical phenomena. In electrostatics for example, the level curves of Φ are the equipotential surfaces, where as the curves of Ψ correspond to lines of flux. In fluid flow, Φ is denoted as the velocity potential and Ψ is referred to as the stream function. This example is of particular interest for our purposes, as we will be specifically making use of the complex potential for our calculation concerning fluid flow in Sec. V.

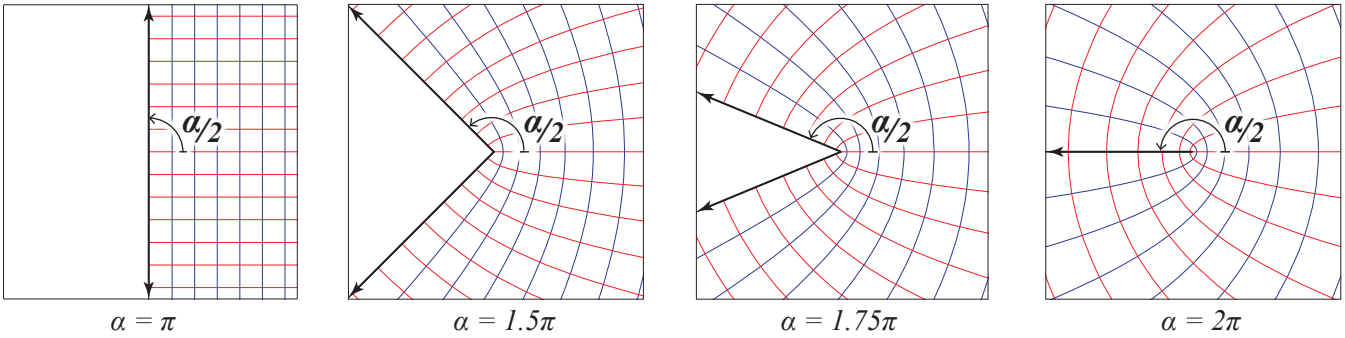

FIG. 2. The Schwarz-Cristoffel transformation $f(\zeta) = \zeta^{\alpha/\pi}$ shown for various values of α. A half plane corresponds to a value of $\alpha = \pi$, and we denote a wedge plane as having an angle of $\pi < \alpha < 2\pi$. In our model of a grain boundary, we will be using the limiting case of $\alpha \to 2\pi$.

D. Conformal Mapping Theory

The importance of a function satisfying the Laplace Equation is that these types of functions are ubiquitous in physical applications. As if often the case, the geometry of the physical domain may not be particularly convenient for obtaining a quick solution to the Laplace Equation. However, we may simplify the process by performing a mapping that serves to transform the Laplace Equation from a convoluted geometry to a simplified one, allowing for an easier solution to be found in the transformed image domain. Afterwards, we may map this solution back to the original, which provides us with the solution corresponding to the more complicated domain we began in.

In order to meet this end, the mappings we choose to use must satisfy the following condition. Consider a mapping in the form of $w = f(\zeta)$ which contains the property $w'(\zeta_0) \neq 0$, then the mapping is referred to as being *conformal*. A conformal mapping is one that preserves the angle between two differentiable arcs meeting at some point ζ_0, such that $f'(\zeta_0) \neq 0$. This allows us to map two orthogonal functions in one plane to another, by which the image functions retain their orthogonality relationship among one another. The importance of this property is clear when considering applying a mapping to a complex potential; the harmonic conjugates comprising of this function must retain their mutual orthogonality in order to uphold any physical reality they correspond to.

It should be mentioned that the function $w = \zeta^{\alpha/\pi}\hat{\boldsymbol{a}}$ is a particular type of mapping, known more formally as a Schwarz-Cristoffel Transformation. As demonstrated in FIG. 2, it has the property of mapping between the half plane and a wedged plane for angles in the range of $\pi < \alpha < 2\pi$. As we approach the limit of $\alpha \to 2\pi$, we note that the wedge becomes an infinitesimally wide slit of semi-infinite length. This particular case is interesting as it provides an excellent model of a grain boundary, both mathematically and physically. Overall, this transformation will be used extensively while deriving H_e in Secs. IV, V, and VI.

E. The Dirichlet And Neumann Problems

We close this section by taking a look at a theorem that provides a basis of validation in our coming application of conformal mappings. While we have already established that a harmonic function undergoing a conformal mapping results in a new function that is harmonic in the mapped domain, it is unknown as to whether or not it will be the unique solution to Laplace's equation within the mapped domain. However, this end may be met by specifying the appropriate boundary conditions our solution must adhere to, which are determined from the physical setup. More specifically, we may specify conditions upon either the harmonic function itself, or the gradient of the function, in order to achieve the guarantee of uniqueness within the region of analysis. Problems of these types have become known as the Dirichlet and Neumann problems, respectively.[3, 4]

The importance of this theorem is that in mapping a solution to the Laplace equation from the half plane to a wedged plane, we can be confident that it is the unique solution corresponding to that plane if it satisfies the specified boundary conditions. Therefore, a solution obtained through a conformal mapping is not only perfectly valid from a physical standpoint, but is also the exact same solution that would have been obtained using an alternative method of approach.

III. ELECTROSTATIC METHOD OF IMAGES

In this section, we take a first look at applying the Schwarz-Cristoffel transformation of $w = \zeta^{\alpha/\pi}$ to simplify an electrostatics method of images problem. To begin, suppose that we wish to solve for the potential corresponding to the shaded region of the w-plane as shown in FIG. 3. This region contains an infinite line charge of charge density $+q$, and is bordered on the u- and v-axes by semi-infinite grounded conducting sheets. Our method of approach will be to transform these two per-

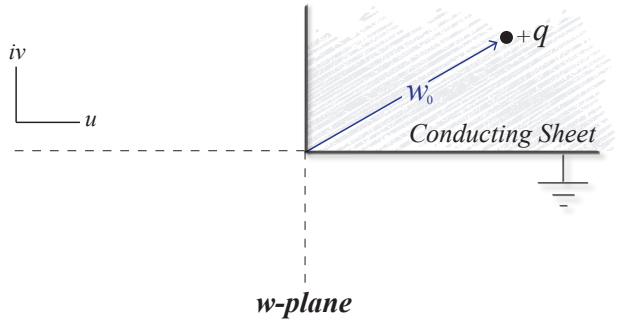

FIG. 3. A line charge of charge density $+q$ positioned at $w_0 = a+\imath b$ from the origin in the $w-$plane, where $w = u+\imath v$. Two semi-infinite, grounded, conducting sheets are positioned along the positive u- and v-axes.

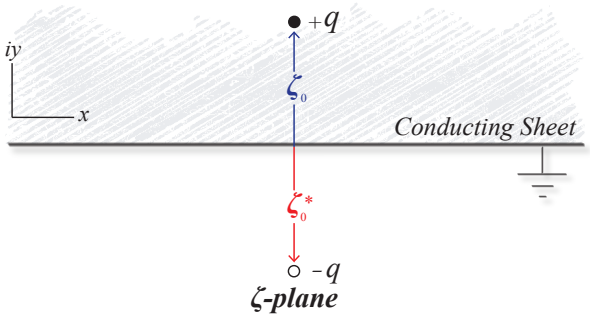

FIG. 4. An infinite line charge of density $+q$ located at ζ_0 above an infinite grounded conducting sheet. The corresponding image line charge of density $-q$ is located at ζ_0^*. V_ζ is only valid within the shaded region of the plane.

pendicular sheets into one planar sheet, which results in an easier geometry to work with in terms of determining the electrostatic potential of the surrounding region. We note that the potential we seek V_w will only be a function of u and v, due to the transnational symmetry of the infinite line charge along the w-axis.

However, we will first determine the potential distribution of an infinite line charge before applying a transformation to this problem. Working in $\mathbb{R}^2$, the electric field of an infinite line charge of charge density $+q$ takes on the form of

$$\boldsymbol{E} = \frac{q}{2\pi\epsilon_0 r}\hat{r} \tag{4}$$

We integrate this expression to obtain the electrostatic potential field distribution, and hence obtain

$$V = -\frac{q}{2\pi\epsilon_0}\ln(r) + c \tag{5}$$

Due to the infinite length of the line charge, there does not exist an infinitely distant reference surface to base the potential from. Therefore, a cylinder with arbitrary radius d centralized along the z-axis is chosen. By setting (5) equal to zero, we solve for the arbitrary constant within and find

$$c = \frac{q}{2\pi\epsilon_0}\ln(d) \tag{6}$$

Therefore, the potential distribution of an infinitely long line charge may be written as

$$V = \frac{q}{2\pi\epsilon_0}\ln\left(\frac{d}{r}\right) \tag{7}$$

Now we are ready to map the wedged w-plane from FIG. 3 onto the half ζ-plane of FIG. 4. This is achieved by substituting the value $\alpha = \pi/2$ into $w = \zeta^{\alpha/\pi}$, giving us

$$w = \zeta^{1/2} \tag{8}$$

In this easier geometry, the method of images now provides a simple solution to the corresponding shaded region of the ζ-plane. With our initial line charge located at ζ_0, the conducting sheet may be replaced by an image line charge of charge density $-q$, residing at the point ζ_0^*. This gives us a potential field distribution of

$$V_\zeta = \frac{q}{2\pi\epsilon_0}\ln\left(\frac{d_\zeta}{|\zeta-\zeta_0|}\right) - \frac{q}{2\pi\epsilon_0}\ln\left(\frac{d_\zeta}{|\zeta-\zeta_0^*|}\right) \tag{9}$$

where by simplifying the logarithm, we arrive at

$$V_\zeta = \frac{q}{2\pi\epsilon_0}\ln\left|\frac{\zeta-\zeta_0^*}{\zeta-\zeta_0}\right| \tag{10}$$

As it is well known that V as given in Eq. (7) satisfies the Laplace equation for $r \neq 0$, the potential distribution determined in Eq. (10) does not at $\zeta = \zeta_0, \zeta_0^*$; therefore, the uniqueness theorem does not apply to the entire shaded region. However, this specific example will still follow, as properties of the natural logarithm will ensure that the correct solution is obtained. Consequently, a transformation of V_ζ into the w-plane will give us the potential distribution V_w corresponding to the shaded region in the w-plane. This inverse transformation is achieved by solving (8) for ζ, giving

$$\zeta = w^2 \tag{11}$$

Then, it follows that by substituting this result into (10), we transform from the ζ-plane back to the w-plane. Thus, we obtain a value for V_w of

$$\begin{aligned} V_w &= \frac{q}{2\pi\epsilon_0}\ln\left|\frac{w^2-w_0^{*2}}{w^2-w_0^2}\right| \\ &= \frac{q}{2\pi\epsilon_0}\ln\left|\frac{(w-w_0^*)(w+w_0^*)}{(w-w_0)(w+w_0)}\right| \end{aligned} \tag{12}$$

Finally, we may expand the logarithm to obtain a solution of

$$\begin{aligned} V_w = \frac{q}{2\pi\epsilon_0}\Bigg(&\ln\frac{d_w}{|w-w_0|} + \ln\frac{d_w}{|w+w_0|} \\ &- \ln\frac{d_w}{|w-w_0^*|} - \ln\frac{d_w}{|w+w_0^*|}\Bigg) \end{aligned} \tag{13}$$

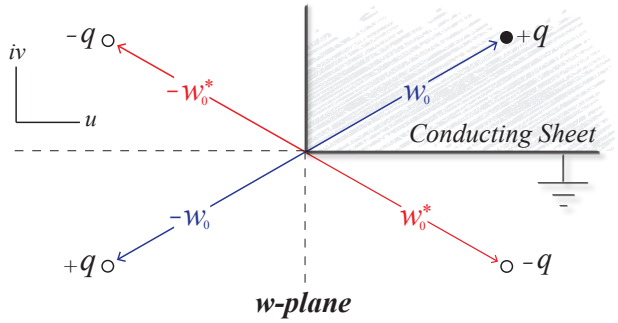

FIG. 5. The method of images solution for an infinite line charge of density $+q$ located between two semi-infinite grounded conducting sheets. The hollow circles represent the image charges. The electrostatic potential, V_w, is only valid in the shaded region of the plane.

The validity of this result may be checked by noting that it also corresponds to a method of images solution applied to the w-plane. This fact becomes clear when observing FIG. 5.

In this particular problem, it would have been much easier to just write down the electrostatic potential V_w by applying the method of images to the problem in the w-plane. However, this method is only viable for two semi-infinite planes that form angles which are integer divisors of 180° [4]. On the other hand, employing a conformal transformation will allow us to solve for a much wider range of configurations than allowed for by the method of images. In this example, we chose to map the entire potential field V from one plane to another. In the following derivation of H_e though, we will only be concerned with how a single point maps. Additionally, a careful setup of our initial coordinate system will allow us to utilize the method of images in solving a problem with respect to angles greater than π.

IV. VORTEX-DEFECT INTERACTION

In this section we begin our derivation of H_e by calculating for the vortex-surface interaction force. Afterwards, a conformal transformation is applied to determine the value of this force in the presence of a grain boundary.

A. Flux Vortex Analogy

By making an analogy between electrostatics and flux vortices, it may be shown that the method of images can be utilized in solving for the interaction force between vortex-defect interactions. Specifically, we examine the case where the interaction distance is much smaller than the London Penetration Depth, such that $r \ll \lambda$. This case is of special interest since this interaction force drops off exponentially for distances on the order of $r \sim \lambda$. If we consider a single flux vortex located at the origin, the two dimensional London equation is written as

$$\nabla^2 h_v - \frac{1}{\lambda^2} h_v = -\frac{\phi_0}{\lambda^2}\delta^2(r) \tag{14}$$

where h_v is the field of a vortex with $\boldsymbol{h} = h_v\,\hat{z}$ and where $\delta^2(r)$ is the two dimensional delta function. However, since we are taking $r \ll \lambda$, the second term on the left may omitted as it is negligibly small in comparison with $\nabla^2 h_v$. This gives us

$$\nabla^2 h_v = -\frac{\phi_0}{\lambda^2}\delta_2(r) \tag{15}$$

which is simply the Poisson Equation in terms of h_v. In comparing this with the Poisson equation for electrostatics, we are able to draw forth the following analogies for the electrostatic potential and effective charge in terms of the flux vortex . Following [5], the term λh_v may be thought of as the electrostatic potential, and the term $\frac{\phi_0}{4\pi\lambda}$ may be considered to be the effective line charge. We specify line charge specifically here, due to the fact that h_v possesses transnational symmetry along the z-axis. Using this analogy, we may write the interaction energy and attraction force between two static vortices in their equivalent electrostatic forms, respectively, as

$$E_{int} = \frac{\phi_0}{4\pi\lambda^2}(\lambda h_v) \tag{16}$$

$$F_{att} = -\frac{\phi_0}{4\pi\lambda^2}\nabla(\lambda h_v) \tag{17}$$

where $F_{att} = -\nabla E_{int}$.

Additionally, boundary conditions will play an essential role in our within our study of vortex-defect interactions. Since the surface between regions of super and non-superconductivity carries a uniform magnetic field, this will be taken as analogous to an equipotential surface from electrostatic problems. Therefore, the surface within a superconductor will be taken as equivalent to a grounded conducting sheet as per our work done in the previous section.

B. Flux Vortex Method Of Images

Further following the condition of $r \ll \lambda$, we may specify an expression common from literature for the magnetic field distribution of a single flux vortex, with

$$h_v = \frac{\phi_0}{2\pi\lambda^2}\ln\frac{\lambda}{r} \tag{18}$$

The derivation of this result can be quite long, but an in-depth presentation for this may be found in [6]. We also quickly note that a function of this form is harmonic, since it satisfies the two-dimensional Laplace equation in $\mathbb{R}^2$. This may be quickly verified by noting the similarity between this expression and that of the potential of an infinite line charge, as determined in Eq. (7).

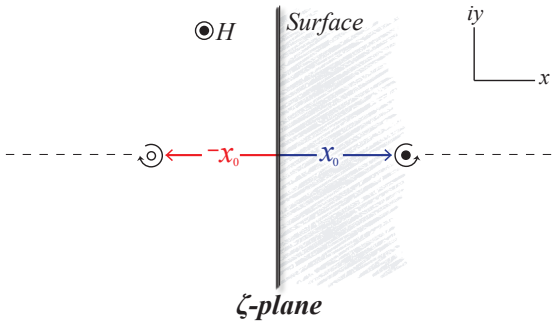

FIG. 6. The method of images solution for a vortex located alongside a superconducting surface. The vortex/anti-vortex positioned at $x_0, -x_0$ respectively are treated by analogy as infinite line charges, and the surface may be considered as a grounded conducting sheet. The internal field H is parallel to the surface.

Moving forward, we will apply the method of images to our established electrostatic-flux vortex analogy in order to solve for the interaction force between a vortex and surface defect. Suppose then, that a vortex is positioned at a distance $\zeta_0 = x_0$ from the planar cavity surface located along the y-axis. Drawing from the analogous electrostatic problem covered in Sec. III, we may solve for the associated scalar potential λh_v by modeling this problem using a vortex and anti-vortex located at x_0 and $-x_0$, respectively, as shown in FIG. 6. Following the expression for h_v from Eq. (18), and by again using $\frac{\phi_0}{4\pi\lambda}$ as the analogous line charge, the magnetic field distribution in the shaded region of the ζ-plane is

$$h_{v,\zeta} = \frac{\phi_0}{2\pi\lambda^2} \ln\left|\frac{\zeta + x_0}{\zeta - x_0}\right| \tag{19}$$

Within a superconductor, the applicable boundary conditions are that the current density $\boldsymbol{j}$ is must be tangential to the surface, and that the magnetic field must constant on the surface. To show that the former holds true, we draw forth another electrostatic-vortex analogy between the current density $\boldsymbol{j}$ and the electric field $\boldsymbol{E} = -\nabla V$, such that

$$\boldsymbol{E} = -\lambda \nabla h_v \tag{20}$$

From magnetostatics, we know that current density may be written as

$$\boldsymbol{j} = \frac{c}{4\pi}(\nabla \times \boldsymbol{h}) \tag{21}$$

In our two-dimensional geometry, this is may be equivalently written as

$$\boldsymbol{j} = \frac{c}{4\pi}\nabla h_v \times \hat{z} \tag{22}$$

Where the above follows from $\boldsymbol{h} = h_v\hat{z}$, since

$$\nabla \times \boldsymbol{h} = -\frac{\partial h_v}{\partial r}\hat{\theta} = \frac{\partial h_v}{\partial r}\hat{r} \times \hat{z} = \nabla h_v \times \hat{z} \tag{23}$$

Hence, drawing forth from (20) and (22), it further follows that $\boldsymbol{j} \cdot \boldsymbol{E} = 0$, since

$$\left(\frac{c}{4\pi}\nabla h_v \times \hat{z}\right) \cdot \left(-\lambda \nabla h_v\right) = 0 \tag{24}$$

This allows us to infer that the lines of current correspond to the equipotential surfaces from the analogous electrostatic problem [5, 7]. Therefore, the condition that $\boldsymbol{j}$ is tangential to the cavity surface is automatically satisfied by (24). Furthermore, Eq. (20) also satisfies our second boundary condition on h_v, due to the fact that $\boldsymbol{E} = -\lambda\nabla h_v$ corresponds to a level curve along the surface of the cavity.

Now that we have satisfied the applicable boundary conditions, we may determine the value of the potential field distribution at the point $\zeta = x_0$ by using (19). The contribution from the image vortex produces a value of

$$h_{v,\zeta} = -\frac{\phi_0}{2\pi\lambda^2} \ln\frac{\lambda}{2x_0} \tag{25}$$

This may equivalently be written as

$$h_{v,\zeta} = -\frac{\phi_0}{2\pi\lambda^2} \ln\frac{\lambda}{r}\bigg|_{r=2x_0} \tag{26}$$

Here we note that this is of the same form as Eq. (18), thereby making it harmonic. Hence, we have shown $h_{v,\zeta}$ to satisfy the Neumann problem corresponding to the shaded region of the ζ-plane. Consequently, a conformal transformation will map $h_{v,\zeta}$ to a harmonic function $h_{v,w}$, which is unique in the shaded region of the w-plane.

Before applying the mapping, we will use the relationships from (16) and (17) along with the value of $h_{v,\zeta}$ from Eq. (25) to write down the interaction energy and force of attraction between the vortex/anti-vortex pair, respectively, as

$$E_{int,\zeta} = -\left(\frac{\phi_0}{4\pi\lambda}\right)^2 \ln\frac{\lambda}{2x_0} \tag{27}$$

$$F_{att\zeta} = -\left(\frac{\phi_0}{4\pi\lambda}\right)^2 \frac{1}{x_0} \tag{28}$$

It is important to note that the given interaction energy is half of what one might expect it to be from equation (16). However, this is due to the fact that only one of the vortices in the problem is real, and therefore the work required to move the real vortex into position is only half as much as is required to move two real vortices into this arrangement. The electrostatic analogy for this may be found in [4].

C. Transforming The Surface

We now wish to determine the interaction force between a vortex and surface defect. We'll achieve this by mapping the expression of $h_{v,\zeta}$ from the ζ-plane of FIG.

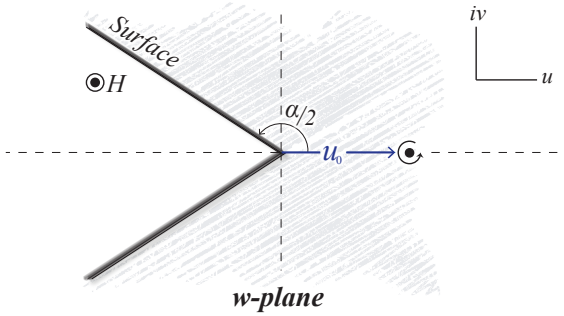

FIG. 7. Modeling a surface defect by using the transformation $w = \zeta^{\alpha/\pi}$. A vortex is positioned on axis with the defect at u_0. The field H is parallel to the surface. No method of images solution exists for this geometry, since $\alpha > \pi$.

6 onto the w-plane of FIG. 7. The wedge produced by using the mapping $w = \zeta^{\alpha/\pi}$ will serve to model the defect, and specifically we'll use it to model a grain boundary in the limit of $\alpha \to 2\pi$. In order to apply the mapping, we must first determine how the variables x, y from the ζ-plane will map to the u, v variables in the w-plane. Consequently, by writing $w = \zeta^{\alpha/\pi}$ in component form, we obtain

$$u + \imath v = (x + \imath y)^{\alpha/\pi} \tag{29}$$

Having conveniently set up our initial coordinate system in the ζ-plane, we need only determine how x maps in order to write $h_{v,\zeta}$ in the w-plane. Therefore, in taking $y = 0$ we have

$$u + \imath v = x^{\alpha/\pi} \tag{30}$$

Here we note that the right hand side consists of only real variables. Therefore, we must have $v = 0$ for the left hand side to retain the equality relationship. This gives us

$$u = x^{\alpha/\pi} \qquad \Longrightarrow \qquad x = u^{\pi/\alpha} \tag{31}$$

Therefore, we may conclude that the point x_0 from the ζ-plane maps to the point $u_0^{\pi/\alpha}$ in the corresponding w-plane. This is all the information we will need to complete our mapping, since we are only concerned with the nature of the magnetic field distribution at one specific point in each plane and not the entire plane itself.

Hence, substituting $x_0 = u_0^{\pi/\alpha}$ into Eq. (25) gives us the magnetic field distribution at the point u_0 of

$$h_{v,w} = -\frac{\phi_0}{2\pi\lambda^2} \ln \frac{\lambda}{2u_0^{\pi/\alpha}} \tag{32}$$

By now using this expression in conjunction with Eqs. (16) and (17) again, we find the interaction energy and interaction force of the vortex-defect pair in the w-plane of

$$E_{int,w} = -\left(\frac{\phi_0}{4\pi\lambda}\right)^2 \ln \frac{\lambda}{2u_0^{\pi/\alpha}} \tag{33}$$

$$F_{att,w} = -\left(\frac{\phi_0}{4\pi\lambda}\right)^2 \frac{\pi}{\alpha u_0} \tag{34}$$

D. Force Comparison

The choice of variables used in each of ζ- and w-planes was arbitrary, and had we chose to, we could have just used the same convention within each plane. This would of course have caused confusion, but nonetheless, the forces we obtained in Eqs. (28) and (34) are directly comparable. To see that this indeed the case, we may just evaluate each expression at the same arbitrary point $x_0, u_0 = r_0$ along the horizontal axis of each respective plane. By doing so, we find that the force of attraction with respect to a wedge shaped defect decreases by a factor of

$$\frac{F_{att,w}}{F_{att,\zeta}} = \frac{\pi}{\alpha} \tag{35}$$

In the limit of $\alpha \to 2\pi$, we find that the interactive force is only half as strong near our modeled grain boundary than it is with respect to a planar surface.

V. THE SINGULAR MAGNETIC FIELD

In order to motivate the following calculations, we will present another important consequence of the previously established flux vortex-electrostatic analogy. Drawing from [5], the Lorentz force exerted upon a vortex in the vicinity of a current is equivalent to the Coulomb force exerted on the analogous line charge. Moreover, in following [1] we find that the edge of a wedge shaped defect results in a singularity within the current density local to that region; hence, the phenomenon of vortex penetration into the bulk of a superconducting medium is expedited. Therefore, we will proceed by calculating for the singular field associated with a wedge shaped defect. Ultimately, this will be used to attain an expression for the corresponding singular current.

A. Fluid Flow Analogy

By neglecting the effects of screening, the problem of the magnetic field distribution is similar to the problem of the potential of the velocity field for an ideal fluid in 2D-geometry. Since the effects of screening the external field are negligible in the case of $r \ll \lambda$, we will adopt this fluid flow analogy in the calculation of the singular field h_s. Consequently, we will consider the flow velocity field

and current density to be parallel and directly analogous to one another, such that $\boldsymbol{v}_f \sim \boldsymbol{j}_s$.

In order to develop an understanding of this analogy, we consider the properties associated with an ideal fluid alongside those inherent of the current density. Ideal fluid flow refers to fluid flow that is steady, inviscid, incompressible, and irrotational. Expanding upon these definitions, steady flow means that our current density be time independent. This we will satisfy by not taking time as a consideration in our derivation. Next, the condition of inviscid flow is automatically satisfied, as it requires no friction to exist between the fluid and surface in contact with the flow. Thirdly, incompressible flow means that the fluid density is constant, which may be written mathematically as $\nabla \cdot \boldsymbol{j}_s = 0$. Since h_s strictly points in the $\hat{z}$ direction, we may write $\boldsymbol{j}_s$ in the form of (21) to satisfy this condition. This gives us

$$\nabla \cdot \frac{c}{4\pi}(\nabla \times \boldsymbol{h}_s) = 0 \tag{36}$$

which follows due to the fact that the divergence of the curl of a vector field is always zero. Finally, irrotational flow means that the curl of the fluid flow is zero. This too is satisfied by writing $\boldsymbol{j}_s$ in the form of Eq. (22). From this we have

$$\nabla \times \frac{c}{4\pi}\nabla h_s \times \hat{z} = 0 \tag{37}$$

which follows since the curl of a gradient is always zero.

At this point, we must point out a slight discrepancy within our analogy that relates fluid flow to the flow of current density. While we have shown that $\boldsymbol{j}_s$ relates to the associated current flow potential, or singular field h_s, as shown in Eq. (22), the flow velocity differs by instead satisfying $\boldsymbol{v}_f = \nabla\Phi$. Therefore, from our relationship of $\boldsymbol{j}_s \sim \boldsymbol{v}_f$, it follows that

$$\nabla h_{s,\zeta} \times \hat{z} \sim \nabla\Phi \tag{38}$$

such h_s is orthogonal to Φ. Nevertheless, we may determine the function corresponding to $h_{s,\zeta}$ by considering the associated complex potential as discussed in Sec. II C.

$$\Omega = \Phi + \imath\Psi \tag{39}$$

Since Ψ is also orthogonal to Φ, we may infer the relationship $h_{s,\zeta} \sim \Psi$. Upon further inspection, we find that these terms are in fact anti-parallel; therefore, it follows that $h_{s,\zeta}$ may be written in terms of Ω as

$$h_{s,\zeta} = \Im(-\Omega) = -\Psi \tag{40}$$

For completeness, we may also express the fluid flow potential under this convention as $\Phi = \Re(\Omega)$, where the symbols $\Im$ and $\Re$ correspond to the taking the imaginary and real parts, respectively.

To verify that this is indeed the case, we refer to Eq. (38) and note that taking cross product with $\hat{z}$ in $\mathbb{R}^2$ is equivalent to multiplying by $-\imath$ in the complex plane. Hence, we apply the gradient and multiply $-\nabla\Omega$ by $-\imath$ before taking the imaginary part in (40) to obtain

$$\nabla h_{s,\zeta} \times \hat{z} \sim \Im(\imath\nabla\Omega) = \nabla\Phi \tag{41}$$

and thus, our assertion is confirmed.

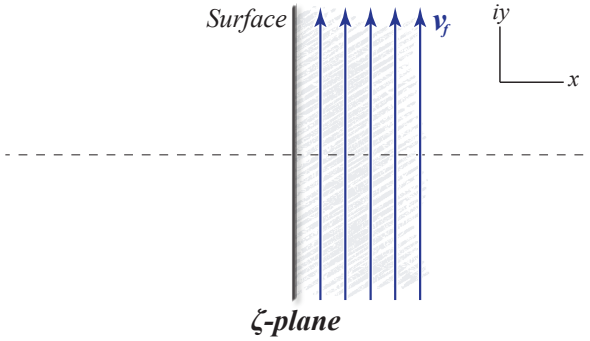

FIG. 8. The flow of an ideal fluid with respect to a planar surface.

B. Flow Along A Plane

There are several ways by which a flow potential of an ideal fluid may be found. Of these, we will follow the theme of this paper and will determine the flow potential around a corner by using a conformal mapping. Consider then, the flow of an ideal fluid over a flat planar surface, as depicted in the in the ζ-plane of FIG. 8. Following this figure, we may write down the flow across the planar surface in complex notation as

$$\boldsymbol{v}_f = \imath A, \qquad \text{for } A \in \mathbb{R} \tag{42}$$

By inspection, it may be seen that this mathematical description adheres to the properties associated with ideal flow. In order to obtain the potential of this velocity field, we'll first solve for the associated complex potential by following the ideas presented in Sec. II C. As per Eq. (3), the complex potential satisfies

$$\Omega'^{*}_{\zeta} = \imath A \tag{43}$$

From this, we may take the complex conjugate of each side and integrate with respect to ζ to obtain

$$\Omega_{\zeta} = -\imath A\zeta \tag{44}$$

Before moving forward with the transformation, we should ensure that all corresponding boundary conditions are met. With respect to an ideal fluid, there must be no flow through the surface of the boundary. This is equivalent to requiring that surface boundary correspond to a streamline, such that the stream function is constant along the boundary. Then, by substituting $\zeta = \pm\imath y$ into (44), we obtain

$$\Omega_{\zeta} = \pm Ar \tag{45}$$

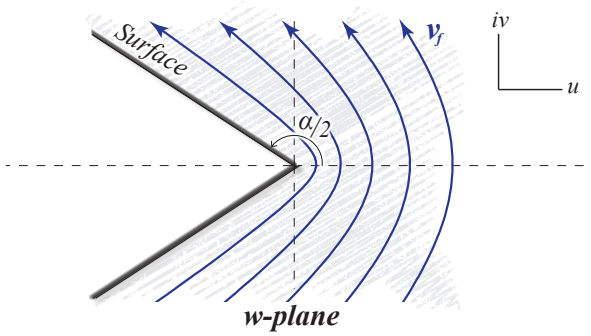

FIG. 9. The flow of an ideal fluid with respect to a wedge shaped surface.

whereby the streamline corresponding to $\Im(\Omega_\zeta)$ equals zero. Then, having fulfilled the requirements of a Neumann problem, we are ready to proceed with the transformation.

C. Flow Around A Corner

As we have done in previous sections, we will model a corner by applying the transformation $w = \zeta^{\alpha/\pi}$ to Ω_ζ, which effectively bringing us from the ζ-plane of FIG. 8 to the w-plane of FIG. 9. In order to accomplish this, we will invert this expression and substitute it into (44) to obtain

$$\Omega_w = -\imath A w^{\pi/\alpha} \tag{46}$$

Written in polar form, with $w = \rho e^{\imath\varphi}$, we have

$$\Omega_w = -\imath A \rho^{\pi/\alpha} e^{\imath\pi\varphi/\alpha} \tag{47}$$

Following (40), we obtain the associated singular field by taking the negative imaginary part of the above, thereby giving us

$$h_{s,w} = A\rho^{\pi/\alpha}\cos\left(\tfrac{\pi}{\alpha}\varphi\right) \tag{48}$$

As a check, we find that our result is consistent with the corresponding solution obtained in [8]. Finally, we may use the form of (22) to express $\boldsymbol{j}_{s,w}$ in terms of the singular field. Accordingly, we have

$$\boldsymbol{j}_{s,w} = -\frac{cA}{4\alpha}\rho^{\pi/\alpha-1}\left(\sin\left(\tfrac{\pi}{\alpha}\varphi\right)\hat{\rho} + \cos\left(\tfrac{\pi}{\alpha}\varphi\right)\hat{\varphi}\right) \tag{49}$$

VI. CALCULATING THE ENTRANCE FIELD

Building upon our work from the previous two sections, we will now conclude our derivation of the entrance field. To continue, we must obtain an estimate for the constant A used in our calculation of the singular field. This may be achieved by considering the total field in the vicinity of the defect, which is

$$H = H_{ext} + h_{s,w} \tag{50}$$

Drawing from the fact that the interaction force decreases exponentially for distances on the order of λ, the estimate for A will be made under the assumption that h_s vanishes at $\rho = \lambda$. Since the singular field is a function of the external field, we account for this as well and take A to be

$$A = -H_{ext}\lambda^{-\pi/\alpha} \tag{51}$$

As we are only concerned with the interaction force along the axis of the defect, we will take $\varphi = 0$ in all subsequent expressions. Then, by substituting A and (48) into (50), we arrive at

$$H = H_{ext}\left(1 - \left(\frac{\rho}{\lambda}\right)^{\pi/\alpha}\right) \tag{52}$$

Moreover, we may also substitute A into (49) to write the singular current near the corner of the defect in terms of the external field. This gives us

$$j_{s,w} = H_{ext}\frac{c}{4\alpha\lambda}\left(\frac{\rho}{\lambda}\right)^{\pi/\alpha-1} \tag{53}$$

Having expressed the singular current as a function of H_{ext}, we may incorporate this term when writing out the Lorentz force, $f_L = \frac{\phi_0}{c} j_\varphi$. Furthermore, since we are specifically concerned with the value of the Lorentz force at the location of the vortex, we will take $\rho = u_0$; hence, we have

$$f_L = H_{ext}\frac{\phi_0}{4\alpha\lambda}\left(\frac{u_0}{\lambda}\right)^{\pi/\alpha-1} \tag{54}$$

Now we recall that as per the established electrostatic analogy, the Lorentz force felt by a vortex is equivalent to the Coulomb force exerted on the synonymous line charge. Therefore, a vortex near a surface will adjust it's position accordingly to balance out the external field and boundary conditions. Then, by equating f_L with $F_{att,w}$ from Eqs. (54) and (34), respectively, we have

$$H_{ext}\frac{\phi_0}{4\alpha\lambda}\left(\frac{u_0}{\lambda}\right)^{\pi/\alpha-1} = \left(\frac{\phi_0}{4\pi\lambda}\right)^2\frac{\pi}{\alpha u_0} \tag{55}$$

From this, it follows that increasing the external field will force the vortex closer to the surface. However, the minimum value this distance takes on is the coherence length ξ, which is the radius of the normal vortex core. Consequently, it follows that H_e corresponds to the value of H_{ext} that causes the vortex to be driven past this minimum value and into the superconducting bulk. As such, H_e may be found by first solving (55) in terms of H_{ext}, giving us

$$H_{ext} > \frac{\phi_0}{4\pi\lambda u_0}\left(\frac{u_0}{\lambda}\right)^{1-\pi/\alpha} \tag{56}$$

Then in taking the limit $u_0 \to \xi$, we determine H_e to be

$$H_e = \frac{\phi_0}{4\pi\lambda\xi}\left(\frac{\xi}{\lambda}\right)^{1-\pi/\alpha} \tag{57}$$

At this point in the derivation, the authors of [2] chose to write the entrance field as

$$H_e \simeq H_c\left(\frac{\xi}{\lambda}\right)^{1-\pi/\alpha} \tag{58}$$

since only the proportionality relationships were desired. However, since we would like to consider this result with respect to Nb_3Sn, we may follow [9, 10] to express the entrance field in a more explicit manner. For $\kappa \gg 1$, we may write the lower and upper critical fields, respectively, as

$$H_{c1} = \frac{H_c}{\sqrt{2}\kappa}\ln\kappa \qquad \text{and} \qquad H_{c_2} = \frac{\phi_0}{2\pi\xi^2} \tag{59}$$

Furthermore, the thermodynamic critical field H_c may be written as

$$H_c = \frac{H_{c_2}}{\sqrt{2}\kappa} \tag{60}$$

Additionally, substituting H_{c2} into the above allows us to write H_c as a function of $\phi_0, \lambda,$ and ξ. Hence, we have

$$H_c = \frac{\phi_0}{2\sqrt{2}\lambda\xi} \tag{61}$$

Therefore, we complete our derivation of H_e by writing the constant term from (57) in terms of H_c, such that

$$H_e = \tfrac{\sqrt{2}}{2}H_c\,\kappa^{\pi/\alpha-1} \tag{62}$$

where $\kappa = \lambda/\xi$ is the Ginzburg-Landau parameter. For completeness, we may also express the entrance field in terms of H_{c1} and H_{c2}, respectively, as

$$H_e = H_{c1}\left(\frac{\kappa^{\pi/\alpha}}{\ln\kappa}\right) = H_{c2}\left(\frac{\kappa^{\pi/\alpha-2}}{2}\right) \tag{63}$$

VII. DISCUSSION

Having obtained a value for the entrance field in our model for a grain boundary, it is important to not only discuss both the validity of this model, but also the implications it has upon using Nb_3Sn as a superconducting surface.

A. Initial Impressions

We begin probing into the validity of (62) by considering it in respect to a planar superconducting surface. This corresponds to a value of $\alpha = \pi$, which allows (62) to be simplified as

$$H_{e,p} = \tfrac{\sqrt{2}}{2}H_c \tag{64}$$

Drawing from [9], the superheating field H_{sh}, which is the maximum value H_e may take on, has been determined to be

$$H_{sh} \approx \tfrac{3}{4}H_c, \qquad \text{for } \kappa \gg 1$$

In the absence of surface defects, we would expect that our model of the entrance field would be equal in value to the superheating field. Therefore, it appears that this determination of H_e agrees well with [9] in regards to a planar surface geometry.

B. Grain Boundary Implications

Now we move to the heart of the matter by evaluating the entrance within the vicinity of a grain boundary. This is achieved by taking the limiting value of $\alpha \to 2\pi$, which turns the surface of the cavity into an infinitesimally thin strip that is semi-infinite in length. In doing so, (62) becomes

$$H_{e,g} = \tfrac{\sqrt{2}}{2}H_c\,\kappa^{-1/2} \tag{65}$$

From a comparison of Eq. (64) with Eq. (65), it follows that

$$H_{e,g} = \kappa^{-1/2}H_{e,p} \tag{66}$$

Therefore, by taking on the value $\kappa \approx 12$ for Nb_3Sn, we obtain

$$H_{e,g} \approx \tfrac{3}{10}H_{e,p} \tag{67}$$

It is known that Nb_3Sn has roughly twice as large of a value for H_c than that of Nb; thus this reduction in entrance field may impair the possibility of using Nb_3Sn as a more efficient superconducting accelerating medium than Nb.

C. Additional Considerations

Since this derivation suggests a potentially significant performance loss within Nb_3Sn, we naturally look to explore the validity of the model used at a deeper level. This first thing we question is in regards to the physical accuracy of using a semi-infinite strip to model a grain boundary, since a grain boundary has a finite length in the real world. However, this aspect of the model remains valid in light of the possible discrepancy. Since the vortex/surface interaction energy falls off exponentially on the order of $r = \lambda$, only a small and finite portion of the semi-infinite strip contributes to the interaction force. Furthermore, this appears to agree with [11],

where it has been found that the entrance field asymptotically approaches a limiting value for distances on the order of $r = 10\xi$. This is further beneficial for our model, as the London Approximation, which is the backbone of our derivation for H_e, is only valid for $r \ll \lambda$. Hence, applying the model to Nb_3Sn with $\kappa \gg 1$ ensures that both previous conditions are satisfied.

Another question that arises concerns the validity of modeling a grain boundary as having an infinitesimal width, as actual grain boundaries are known to have widths on the order of ξ. Since the drop in entrance field was drastic in going from a planar to infinitesimal grain boundary strip, it would appear worthwhile to recreate the derivation of H_e using a more complicated conformal transformation that incorporates a width dimension. Numerical calculations in [11] show that H_e drops dramatically for defect widths in the range of 0 to 2ξ, and asymptotically level out for widths greater than 2ξ. In light of this, we would expect that the drastic reduction in H_e obtained in our derivation to be an overestimate of the reduction that occurs in the vicinity of a real grain boundary.

Finally, we may also consider as to what end neglecting the effects of screening ultimately had in our calculation of H_e. A study regarding this has been conducted in [1], from which the authors have concluded that the value of H_e in the vicinity of a thin crack is instead

$$H_{e,g} = \sqrt{\pi}\kappa^{-1/2} H_{e,p} \tag{68}$$

In comparing the above to (66), we find there to be a substantial difference between the given expressions. In regards to Nb_3Sn, this result suggests that

$$H_{e,g} \approx \tfrac{1}{2} H_{e,p} \tag{69}$$

While this is an improvement over what was found in (67), the reduction in magnitude is still significantly large with respect to the outlook of utilizing Nb_3Sn in the construction of superconducting accelerators.

VIII. CONCLUSION

We have examined a possible drawback of using Nb_3Sn as a superconducting surface in radio-frequency applications. Since Nb_3Sn is a type-II superconductor, the metastable vortex state is exhibited in transitioning from the Meissner to normal state with increasing surface magnetic field. While it is energetically favorable for flux vortices to enter a superconducting surface in the vortex state, the Bean-Livingston barrier prevents this penetration from occurring until the external applied field surpasses the entrance field. However, due to the relatively small coherence length of Nb_3Sn, it has been theorized that surface defects may serve to diminish the value of the entrance field. Following a derivation given in [2], a mathematical model of a grain boundary defect has been created through the utilization of techniques from complex analysis. Specifically, a conformal mapping has been applied to a planar surface geometry such that a new surface geometry analogous in effect to a grain boundary has been created.

Using this technique, vortex-defect interaction forces on orders of distances that allow for use of the London approximation were examined. Consequently, it has been found that the entrance field in the presence of a grain boundary is roughly four times smaller in value than in the case of a planar surface. This result suggests that Nb_3Sn will be very susceptible to surface defects in the form of grain boundaries, and may ultimately fail to outperform Nb. However, since this model only roughly resembles an actual grain boundary, further study of this problem through the use of more complicated mappings should be considered.

ACKNOWLEDGMENTS

I would like to thank Sam Posen and Matthias Liepe for their guidance and support throughout my research this summer, as well the National Science Foundation for their generous grant which made this work possible.

[1] A. Aladyshkin, A. Mel'nikov, I. Shereshevsky, and I. Tokman, Physica C: Superconductivity **361**, 67 (2001).
[2] A. Buzdin and M. Daumens, Physica C: Superconductivity **294**, 257 (1998).
[3] M. J. Ablowitz and A. S. Fokas, *Complex Variables: Introduction and Applications* (Institute of Physics Publishing, London, 2003).
[4] D. J. Griffiths, *Introduction to Electrodynamics* (Addison Wesley, New Jersey, 1999).
[5] A. Buzdin and D. Feinberg, Physica C: Superconductivity **256**, 303 (1996).
[6] P. D. Gennes, *Superconductivity of Metals and Alloys* (Benjamin, New York, 1996).
[7] A. Buzdin and M. Daumens, Physica C: Superconductivity **332**, 108 (2000).
[8] L. D. Landau and E. Lifshitz, *Fluid Mechanics* (Pergamon Books Ltd., New York, 1987).
[9] H. Padamsee, J. Knobloch, and T. Hays, *RF Superconductivity for Accelerators* (Wiley-VCH, Canada, 2008).
[10] A. S. Alexandrov, *Theory of Superconductivity: From Weak to Strong Coupling* (Cambridge University Press, Cambridge, 2003).
[11] D. Y. Vodolazov, Phys. Rev. B **62**, 8691 (2000).